Optical patterns with different wavelengths

G. Kozyreff*
Oxford Centre for Industrial and Applied Mathematics, Oxford University, Oxford, OX1 SLB, United Kingdom

M. Tlidi†
Optique Nonlinéaire Théorique, Université Libre de Bruxelles, Campus Plaine, C.P. 231, 1050 Bruxelles, Belgium
(Received 16 October 2003; revised manuscript received 9 February 2004; published 2 June 2004)

The semiconductor resonator is an example of an optical system where two modulational instabilities with different wave numbers coexist. In the limit of nascent bistability, the dynamics is generically described by a nonvariational real order parameter equation, of which we give a detailed derivation. This considerably simplifies the linear and weakly nonlinear stability analyses. When the two instabilities are close together, we derive normal form equations and put special emphasis on "envelope" branches of solutions. These particular solutions may connect the two instability points or form an isola. On the basis of these rigorous results, we finally discuss the case of distant modulational instabilities, in both one and two transverse dimensions.

DOI: 10.1103/PhysRevE.69.066202 PACS number(s): 05.45.−a, 42.65.Sf

I. INTRODUCTION

Over the last 20 years, several theoretical and experimental studies have investigated the coupling between nonlinearity, dissipation, and diffraction. This coupling allows for the formation of transverse dissipative structures, which are widely observed in nonlinear optical systems. These phenomena are common to many nonequilibrium systems [1–6]. In optics, early reports on transverse structures were given in [7,8], which described pulses propagation in bistable systems. Later on, it was shown that the existence of transverse patterns does not require bistable homogeneous steady states. They were analyzed analytically in the mean-field approximation, within what is now often called the Lugiato-Lefever (LL) model [9]. In that work, a connection was established between transverse optical patterns and the well-known Turing instability in reaction-diffusion systems [10] (otherwise called modulational instability). These transverse optical structures can be stationary or time dependent, spatially periodic or localized in the plane orthogonal to the propagation direction of the beam. They have also been studied under the influence of the walk-off [11], advection [12], and beyond the mean-field limit [13]. They result from a modulational instability (MI) which is responsible for the transition to a self-organized or ordered state where translational symmetry is broken along one or more directions. This subject has been abundantly discussed in a number of overviews [14–24].

However, these systems are often subjected to successive instabilities and mode interaction may alter the self-organization process. For example, MI and Hopf branches of solutions may loose their stability under their mutual interaction, giving rise to a mixed-mode solution [25]. In passive cavities and frequency conversion systems, the interaction between MI's and saddle-node bifurcations may influence the existence and stability of the emerging structures [26,27], while in all-fiber bistable ring cavities, it may strongly affect the switching dynamics [28] (in that system, diffraction is replaced by chromatic dispersion).

In this paper, we present analytical results on the interplay between two MI's with different wavelengths. This completes a previous communication on the question [29] and, to some extent, complements a numerical investigation in [30,31]. An important physical application of this study is given by semiconductor resonators. These devices have potential use in information technology and so have received special attention in recent years. In this context, the formation of periodic patterns and localized structures has been the subject of detailed studies [32–36]. Again, these dynamical behaviors are ultimately related to MI, as shown on general grounds [37] and proved recently for semiconductor cavities [38]. However, such is the complexity of this system that even the linear stability analysis of the homogeneous solution is generally done numerically; besides, it is commonly believed that no further analytical treatment is possible. Hence, despite all experimental and numerical work done on this problem, there is only little analytical understanding about this system. More generally, one expects the coexistence of two MI's with different wavelengths to be a frequent dynamical situation; it was, for instance, recently reported in the theory of vegetation patterns [39]. These considerations motivate the present work.

By considering the weakly nonlinear dynamics near the nascent optical bistability regime, we derive a real order parameter equation. This equation is generic for the limit of nascent bistability and contains as a particular case the Swift-Hohenberg equation, which regularly shows up in nonlinear optics [40–42]. It can also be derived, for instance, for the liquid-crystal light valve [43]. It is the simplest possible model featuring bistability and two MI's with different critical wave numbers. Unlike the Swift-Hohenberg equation, though, it is generally nonvariational, so that there is no Lyapunov functional or "potential" to minimize. Next, we derive a normal form equation describing the interaction between two neighboring MI's. The present analysis differs

*Electronic address: kozyreff@maths.ox.ac.uk
†Electronic address: mtlidi@ulb.ac.be; URL: http://www.ulb.ac.be/sciences/ont

from most, if not all, previous studies on the subject, which investigate resonant combinations of critical wave numbers. For instance, it has been shown that the interaction between Turing instabilities with different wavelengths leads to the formation of quasicrystals and superlattices [44]. In the present case, an infinity of branches of periodic solutions arises and it is crucial to consider the envelope of these branches in the bifurcation diagram.

In the next section, we briefly introduce the model of the semiconductor cavity. The derivation of the real order parameter equation is presented in Sec. III. In Sec. IV, the limit where the two instability points are close together is investigated for one transverse dimension. In Secs. V and VI, we extend our analysis to distant instabilities and to two transverse dimensions. Finally, we conclude in Sec. VII.

II. DESCRIPTION OF THE MODEL

Our starting point is the model put forward in [33]. However, the variables are rescaled with respect to the lasing threshold (in the absence of injected field), rather than the transparency values, because it reduces the number of free parameters.

Consider a bulk semiconductor cavity driven by a constant electric field amplitude Y at frequency ω_i. The dynamical equations for the dimensionless field F and carrier (real) variable Z are

$$\frac{\partial F}{\partial t} = i\theta F + (1 + i\alpha)ZF - i\nabla^2 F + Y, \tag{1}$$

$$\frac{\partial Z}{\partial t} = \gamma[P - Z - (1 + 2Z)|F|^2 + D\nabla^2 Z]. \tag{2}$$

Time and space have been rescaled to the photon lifetime κ^{-1} and the diffraction length $\ell = c/\sqrt{2\kappa\omega_i}$. In the first equation, $\theta = (\omega_c - \omega_i)/\kappa$ is the normalized cavity detuning, α is the linewidth enhancement factor, and ∇^2 is the transverse Laplacian. In the second equation, $\gamma = 1/\kappa T_n$ is the ratio of the photon lifetime to the nonradiative carrier recombination time while $D = D_Z T_n/\ell^2$ is the normalized carrier diffusion constant. Finally, P is the pump parameter; it is related to the injected current I through $P = (gN_{th}/2\kappa)(I/I_{th} - 1)$, where g is the differential gain and N_{th} and I_{th} are the lasing threshold values of the electron density and the electric current, respectively. They are themselves related to the transparency density N_0 and the volume of the active region V through $N_{th} = N_0 + \kappa/g$ and $I_{th} = eVN_{th}/T_n$. In what follows, we only consider pumping currents below the lasing threshold, so that $-gN_{th}/2\kappa < P < 0$. For the sake of simplicity, we have neglected the radiative recombination of carriers and, without loss of generality, Y is real.

In the case of a multi-quantum-well (MQW) structure, light and matter can interact through a well-resolved excitonic line. Below the band gap, this line is reasonably well described by a Lorentzian profile with central frequency ω_e and half width γ_e. With the reduced detuning $\Delta = (\omega_e - \omega_i)/\gamma_e$, Eq. (1) should then be modified to

$$\frac{\partial F}{\partial t} = i\theta F + \frac{1 + i\Delta}{1 + \Delta^2} ZF - i\nabla^2 F + Y. \tag{3}$$

The system (1), (2) can be transformed into (2), (3) by the substitutions $\alpha \to \Delta$, $\theta \to (1+\Delta^2)\theta$, $D \to D/(1+\Delta^2)$, and $Y \to (1+\Delta^2)Y$ and a trivial rescaling of space and time. Any result obtained for the bulk semiconductor material can therefore be transposed to the MQW by these substitutions. Bearing this in mind, we will focus hereafter on the bulk semiconductor structure.

III. REDUCTION OF THE MODEL

The dynamics of a coherently driven semiconductor cavity is characterized by hysteresis and modulational instabilities — the latter giving rise to either periodic or localized distribution of light intensity in the near field. In order to construct a simplified, yet as complete as possible picture of this dynamics, one should look for conditions where (i) the bistability is nascent, (ii) the MI's that are responsible for the appearance of localized structures and other spatially periodic patterns are in a close vicinity of the switching region, and (iii) the associated unstable wave numbers k are small (see [18,40], where the same considerations are applied to two-level atoms media).

A. Limit of small cavity detuning

When $\theta = 0$, the homogeneous stationary solution of Eqs. (1) and (2) is implicitly given by

$$Y = -(1 + i\alpha)\frac{P - |F|^2}{1 + 2|F|^2} F, \tag{4}$$

with the constraint that Y be real. Nascent bistability corresponds to $\partial Y/\partial|F| = \partial^2 Y/\partial|F|^2 = 0$ and is reached with

$$F_c = (1 - i\alpha)\left(\frac{3/2}{1 + \alpha^2}\right)^{1/2}, \quad Z_c = -3/2,$$
$$P_c = -9/2, \quad Y_c = \left(\frac{1 + \alpha^2}{8/27}\right)^{1/2}. \tag{5}$$

At this critical point, the characteristic polynomial has the form

$$P(\lambda, k) = \lambda^3 + a_{1,k}\lambda^2 + a_{2,k}\lambda + a_{3,k}, \tag{6}$$

where k is the wave number of a perturbation and

$$4a_{3,k} = \gamma k^2\{D[9 + (2k^2 - 3\alpha)^2] + 8(2k^2 - 3\alpha)\}. \tag{7}$$

$\lambda = 0$ is a root of the characteristic polynomial if $a_{3,k}$ vanishes. This occurs for $k = 0$, but also with $0 < k \ll 1$ provided that

$$D \simeq D_c = \frac{8\alpha/3}{1 + \alpha^2}. \tag{8}$$

With this piece of information, we are in a position to reduce the laser model to a single, scalar partial differential equation by perturbation analysis. To formalize the requirement of a

small hysteresis domain, we introduce a small parameter ϵ by

$$P = P_c + 3\epsilon^2 p. \tag{9}$$

We then expand Y, D, and θ as

$$Y = Y_c(1 + \epsilon^2 y_2 + \epsilon^3 y/4 + \cdots), \tag{10}$$

$$D = D_c(1 + \epsilon d + \cdots), \tag{11}$$

$$\theta = \epsilon^3 \bar{\theta}/D_c. \tag{12}$$

In the small-k limit, one root of the characteristic polynomial is asymptotically given by $\lambda \sim -a_{3,k}/a_{2,k} \sim -\frac{1}{4}\gamma k^4/a_{2,k}$. This suggest to rescale time and space as $\tau \sim \epsilon^2 t$ and $\boldsymbol{\xi} \sim \epsilon^{1/2}\mathbf{x}$ and it is convenient to set

$$\tau = \frac{\epsilon^2 t}{1/\gamma + D_c/\alpha}, \quad \boldsymbol{\xi} = \frac{\epsilon^{1/2}\mathbf{x}}{\sqrt{D_c}}. \tag{13}$$

We can now write the following asymptotic expansion for F and Z in Eqs. (1) and (2):

$$F(\mathbf{x},t) = F_c[1 + \epsilon f(\boldsymbol{\xi},\tau) + \epsilon^2 f_2(\boldsymbol{\xi},\tau) + \cdots], \tag{14}$$

$$Z(\mathbf{x},t) = Z_c[1 + \epsilon z(\boldsymbol{\xi},\tau) + \epsilon^2 z_2(\boldsymbol{\xi},\tau) + \cdots]. \tag{15}$$

Collecting like powers of ϵ, we find, at dominant order

$$-f - z = 0, \tag{16}$$

$$f + f^* + 2z = 0. \tag{17}$$

This immediately yields $z = -f$. We note for future reference that if the system above were inhomogeneous, solvability would require that the sum of Eq. (16) with its complex conjugate and Eq. (17) vanish.

At order ϵ^2, we have

$$-f_2 - z_2 = -y_2 - f^2 + \frac{i+\alpha}{4\alpha}\nabla^2 f, \tag{18}$$

$$f_2 + f_2^* + 2z_2 = -p + 2f^2 - \frac{1}{2}\nabla^2 f, \tag{19}$$

where ∇^2 means now $\partial^2/\partial\xi_1^2 + \partial^2/\partial\xi_2^2$. The solvability condition for this pair of equations is $y_2 = -p/2$ and the solution at this order is

$$f_2 = \frac{-i}{4\alpha}\nabla^2 f, \quad z_2 = f^2 - \frac{p}{2} - \frac{1}{4}\nabla^2 f. \tag{20}$$

Finally, by substituting this solution in the next order and applying the solvability condition, we get the following scalar equation for the field variable f:

$$\frac{\partial f}{\partial \tau} = y + \bar{\theta} - f(p + f^2) + (d - f/2)\nabla^2 f - a\nabla^4 f - \nabla^2 f^2. \tag{21}$$

This is the real order parameter equation for the semiconductor cavity. The nonlinear diffusion terms $f\nabla^2 f$ and $\nabla^2 f^2$ render it nonvariational. They do not arise in the study of two-level atoms where diffusion is neglected and small detunings are assumed [18]. Hence, they are directly imputable to the diffusion of charge carriers and to the $O(1)$ value of the α parameter. We find that an equation of the form (21) naturally arises when studying other pattern-forming systems under the conditions (i)—(iii) mentioned above [43], which gives it a generic character. Let us mention that real order parameter equations with nonlinear diffusive terms have been derived earlier for optical parametric oscillators [42,45,46] and thermal convection [47]; however, they preserve the inversion symmetry.

Let us examine the various parameters entering this equation. First, we see that for small cavity detunings, the reduced detuning $\bar{\theta}$ and driving strength y play the same role. The new pump parameter p determines whether the system is monostable ($p > 0$) or bistable ($p < 0$) and controls the magnitude of the hysteresis. Next, d is an overall diffusion coefficient; it can be negative if diffraction dominates diffusion. Finally, the reduction to Eq. (21) is physically relevant only if the coefficient a is positive. Otherwise, fluctuations with arbitrarily large wave number would be unstable and the scaling we used for the spatial dependence becomes inappropriate. In the present limit of a vanishing detuning, it is given by

$$a \equiv \frac{1 - \alpha^2}{4\alpha^2}. \tag{22}$$

Therefore, the linewidth enhancement factor α should be less than 1. However, this restriction can be lifted if θ is allowed to vary more substantially, as we explain in Sec. III C.

B. Comparison with original model

The derivation of Eq. (21) relies on the smallness of the parameter ϵ in Eq. (9) and it is important to assess how small this parameter must be to faithfully reproduce the dynamics of the original equations (1) and (2). To this end, let us compare the linear stability analysis of the two models.

In the reduced model, the homogeneous steady state is given by

$$y = f_s(p + f_s^2), \tag{23}$$

while perturbations of the form $\exp(\lambda\tau + i\mathbf{k}\cdot\boldsymbol{\xi})$ around f_s satisfy the dispersion relation

$$\lambda = -p - 3f_s^2 - (d - 5f_s/2)k^2 - ak^4. \tag{24}$$

Equating simultaneously λ and $\partial\lambda/\partial k$ to zero, the thresholds for MI's are then found to be

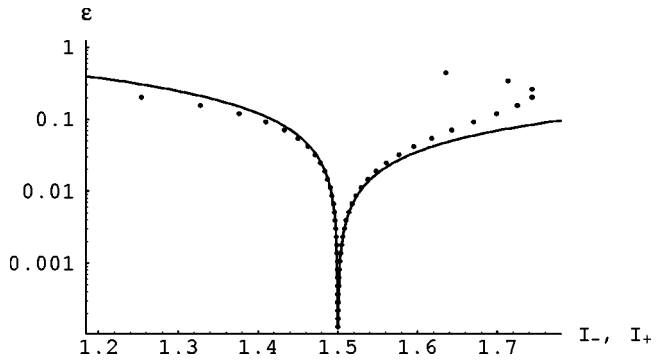

FIG. 1. Threshold intensities $I_\pm$ predicted with the original model (dotted line) and the reduced model (solid line) as a function of the smallness parameter ϵ. Reduced parameter values $p=1$, $d=-5$, $a=3.75$.

$$f_s = f_\pm = \frac{10d \pm 4\sqrt{a[12d^2 + (25-48a)p]}}{25-48a}, \tag{25}$$

giving the injection thresholds

$$y = y_\pm = f_\pm(p + f_\pm^2). \tag{26}$$

The associated critical wave numbers

$$k_\pm = \left(\frac{5f_\pm - 2d}{4a}\right)^{1/2} \tag{27}$$

are real provided that $5f_\pm > 2d$. In terms of the original variables, the threshold field amplitudes for MI's are $F_\pm = F_c(1 + \epsilon f_\pm)$, but since F_c is complex, it is more convenient to consider the intensities

$$I_\pm = |F_c|^2(1+\epsilon f_\pm)^2 = \frac{3}{2}(1+\epsilon f_\pm)^2. \tag{28}$$

In Fig. 1, we compare these intensity thresholds with those obtained by numerically solving the characteristic polynomial of Eqs. (1) and (2). We choose a set of parameters p, d, and a for which two MI's exist and find very good agreement even for moderately small values of ϵ. In fact, the two models only start to disagree at $\epsilon \simeq 0.2$, when $D = D_c(1+\epsilon d)$ becomes negative, hence physically irrelevant. In Fig. 2, the branches of bifurcating solutions are compared for the same parameter set and $\epsilon = 0.05$. Here, too, the agreement is very encouraging. However, we note that ϵ sometimes has to be much smaller for other sets of parameters.

C. Arbitrary cavity detuning

A vanishingly small cavity detuning θ is rarely, if ever, achieved in practice. It is therefore important to show that the possibility of real order parameter description such as Eq. (21) does not critically rely on this assumption. We now outline the derivation when θ is significantly large. Similarly to expression (4), one can still write $Y = Y(\theta, P, |F|)$. Nascent bistability requires that both $\partial Y/\partial|F|$ and $\partial^2 Y/\partial|F|^2$ vanish, which yields the critical parameter values $P_c(\theta)$ and $Y_c(\theta)$ and field amplitude $F_c(\theta)$. From the characteristic polynomial evaluated at this point, one then finds a condition $D \simeq D_c(\theta)$ for the occurrence of a long-wavelength instability. In practice, for a given D, the cavity detuning θ can be tuned so as to have $D - D_c(\theta)$ small.

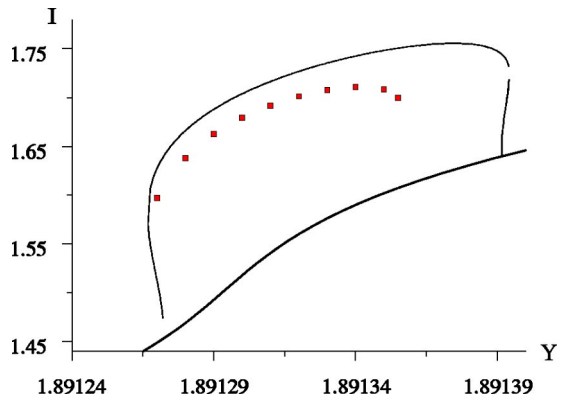

FIG. 2. Numerical bifurcation diagram computed with one transverse dimension with reduced (thin line) and original model (squares). The thick line is the homogeneous state. The parameters are the same as in Fig. 1 and $\epsilon = 0.05$. In the full model, $P=-4.4925$, $D=0.470625$, $\alpha=0.25$. The reduced model slightly overestimates the top MI point, consistently with Fig. 1. Both models predict subcritical bifurcation.

In the absence of explicit formulas for F_c, Z_c,... one has to compute these values numerically for each pair of α and θ. Then the same perturbation expansion as in Sec. III A can be carried out. At the end of the day, the model equations (1) and (2) always reduce asymptotically to the form

$$\frac{\partial f}{\partial \tau} = \mathcal{A}_1 - f(\mathcal{A}_2 + \mathcal{A}_3 f^2) + (\mathcal{A}_4 - \mathcal{A}_5 f)\nabla^2 f - \mathcal{A}_6 \nabla^4 f - \mathcal{A}_7 \nabla^2 f^2, \tag{29}$$

where the coefficients $\mathcal{A}_i$ are functions of θ and depend on the parameter deviations y, p, and d in the same way as in Eq. (21). In particular, $\mathcal{A}_6$ depends only on α and θ. The domain of validity of Eq. (29) is therefore bounded by the constraint

$$\mathcal{A}_6(\alpha, \theta) > 0. \tag{30}$$

We have computed this coefficient numerically and drawn the locus $\mathcal{A}_6(\alpha,\theta)=0$ in the (α,θ) plane in Fig. 3. The domain of validity of Eq. (29) is above this line. As an example, let us consider the following typical parameter values: $D_Z = 30\ \mathrm{cm^2\ s^{-1}}$, $\gamma_\parallel = 10^9\ \mathrm{s^{-1}}$, $\kappa = 5\times 10^{11}\ \mathrm{s^{-1}}$, $\omega_i = 2.2 \times 10^{15}\ \mathrm{s^{-1}}$, and $\alpha = 3$. The corresponding normalized diffusion parameter D equals 0.67, and we find that it is close to $D_c(\theta)$ provided that $\theta \simeq 1.66$, which falls in the validity domain.

Having calculated the curve $\mathcal{A}_6(\alpha,\theta)=0$ for the bulk semiconductor material, a simple rescaling of the axes suffices to draw the corresponding curve $\mathcal{A}_6(\Delta, (1+\Delta^2)\theta)=0$ for the MQW system. As can be seen, the domain of validity is markedly increased for large detunings Δ from the excitonic resonance.

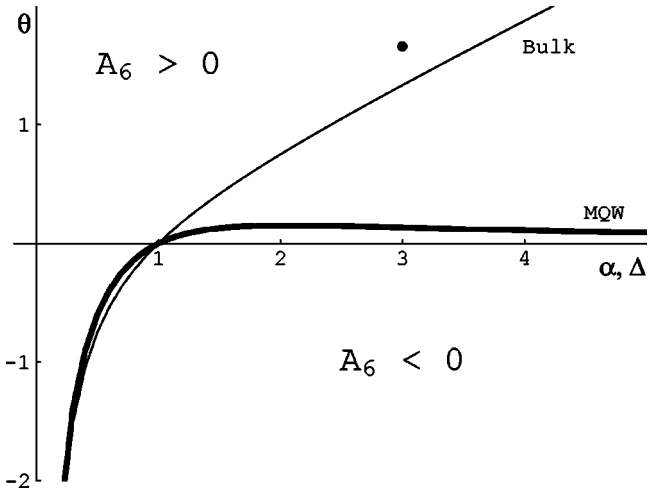

FIG. 3. Curves $\mathcal{A}_6(\alpha,\theta)=0$ and $\mathcal{A}_6(\Delta,(1+\Delta^2)\theta)=0$ above which Eq. (29) is valid for the bulk and MQW materials, respectively. The spot corresponds to the numerical example given in the text.

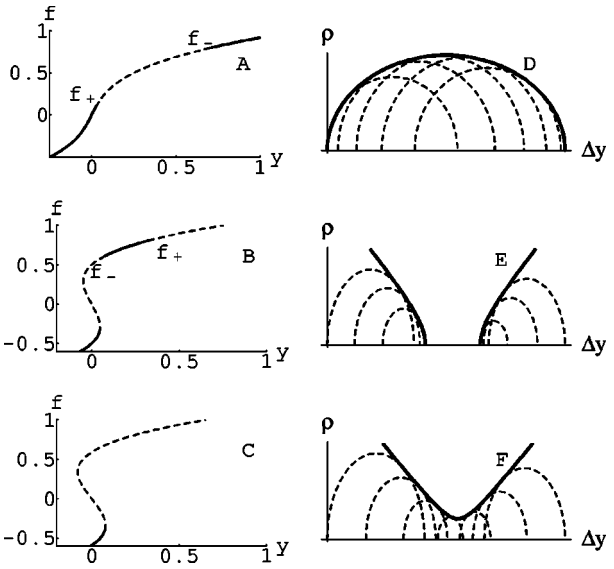

FIG. 4. (A), (B), (C) Three possible outcomes of the linear stability analysis of the homogeneous state of Eq. (21). Dotted lines indicate unstable regions. The limit $p\to p_c$ corresponds to $f_+\to f_-$ in (A) and (B), leading either to a completely stable or completely unstable branch of homogeneous solutions. (D), (E), (F) branches of periodic solutions. From top bottom: $\Delta p<0<(\mathcal{D}-1)$, $(\mathcal{D}-1)<0<\Delta p$, and $(\mathcal{D}-1),\Delta p<0$. Dashed line: branches of periodic solutions with fixed wave number Δk. Thick line: "envelope" branch of the periodic solution.

The reduced model (21) is almost as general as Eq. (29). The former, however, is more informative because the effect of the parameter deviations y, p, and d on the dynamics is directly apparent. From now on, we will therefore restrict our discussion to θ, $\overline{\theta}=0$; otherwise, y, p, and d would appear at the same places in Eq. (29), preceded by some θ-dependent coefficients.

IV. INTERACTION BETWEEN INSTABILITIES

As revealed by the linear stability analysis, two MI can destabilize the homogeneous state. Two possible situations where both thresholds simultaneously exist are depicted schematically in Fig. 4. The bifurcating branches of solution inevitably interact. Such an interaction between two MI's is generally investigated when the associated critical wave numbers are equal or commensurate. Neither of the two situations apply here for k_+ and k_-. However, inspection of Eq. (25) reveals that, when

$$p\to p_c=\frac{12d^2}{48a-25}, \tag{31}$$

the two MI points f_-, f_+ tend to a common value

$$f_c=\frac{-5p_c}{6d}, \tag{32}$$

while

$$y_-,y_+\to y_c=f_c(p_c+f_c^2), \tag{33}$$

$$k_-,k_+\to k_c=\left(\frac{12f_c}{5}\right)^{1/2}. \tag{34}$$

In the vicinity of the critical point where the two bifurcations coincide, we may undertake a weakly nonlinear analysis. The simple form of Eq. (21) makes the task easier but this could be done with the original model as well. Here, we only study the problem in one dimension. To this end, we introduce a new small parameter $\overline{\epsilon}$, which measures the distance from the critical point, and two bifurcation parameters Δp and Δy as

$$p=p_c+3\overline{\epsilon}^2\Delta p, \tag{35}$$

$$y=y_c+\overline{\epsilon}ak_c^4\Delta y, \tag{36}$$

where the factors in front of Δp and Δy are there to ease subsequent algebraic manipulations. Next, in the spirit of multiple-scale analysis, we write the following perturbation expansion for f:

$$f=f_c+\overline{\epsilon}\phi_1(\xi,\tau;\eta,\sigma)+\overline{\epsilon}^2\phi_2(\xi,\tau;\eta,\sigma)+\cdots, \tag{37}$$

with the new time and space scales

$$\sigma=3\overline{\epsilon}^2\tau,\quad \eta=6\overline{\epsilon}\xi/5k_c. \tag{38}$$

Substituting this development into Eq. (21) and grouping terms of like powers in $\overline{\epsilon}$, we find at order $\overline{\epsilon}$

$$\frac{\partial\phi_1}{\partial\tau}=\mathcal{L}(\phi_1-\Delta y), \tag{39}$$

where $\mathcal{L}$ is a differential operator defined as

$$\mathcal{L}=-a\left(k_c^2+\frac{\partial^2}{\partial\xi^2}\right)^2. \tag{40}$$

As $\tau\to\infty$, the solution of this equation tends to

$$\phi_1 = \Delta y + [A(\eta,\sigma)\exp(ik_c\xi) + \text{c.c.}], \tag{41}$$

where A is the amplitude of the modulated field and "c.c" stands for "complex conjugate." At order $\bar{\epsilon}^2$, the equation is

$$\frac{\partial \phi_2}{\partial \tau} = \mathcal{L}\phi_2 - \frac{5}{4}k_c^2(\Delta p + \Delta y^2) - \frac{3}{2}k_c^2|A|^2 + \frac{13}{4}k_c^2[A^2\exp(2ik_c\xi) + \text{c.c.}], \tag{42}$$

and its solution is given by

$$4ak_c^2\phi_2 = -5(\Delta p + \Delta y^2) - 6|A|^2 + \frac{13}{9}[A^2\exp(2ik_c\xi) + \text{c.c.}]. \tag{43}$$

Finally, at order $\bar{\epsilon}^3$, we obtain an equation of the form

$$\frac{\partial \phi_3}{\partial \tau} = \mathcal{L}\phi_3 + \sum_{n=-3}^{3}[\mathcal{M}_n\exp(nik_c\xi) + \text{c.c.}]. \tag{44}$$

We then have the solvability condition that the resonant term $\mathcal{M}_1$ vanish in order for ϕ_3 not to diverge. This yields the normal-form equation

$$\frac{\partial A}{\partial \sigma} = A(-\Delta p - \Delta y^2 - l|A|^2) - 2i\Delta y\frac{\partial A}{\partial \eta} + \mathcal{D}\frac{\partial^2 A}{\partial \eta^2}, \tag{45}$$

where

$$l = 1 - \frac{13}{54a}, \quad \mathcal{D} = \frac{48a}{25}. \tag{46}$$

As generally expected for MI's, the normal form is a Ginzburg-Landau equation. In it, the interaction between the two instabilities manifests itself in two ways. First, two parameters Δp and Δy are necessary to describe the bifurcation; i.e., it is of codimension 2 (see, for instance, [48]). Second, the way in which these bifurcation parameters appear in the amplitude equation is quite distinct from the standard, isolated MI. Particularly interesting is the complex first-order partial derivative multiplied by Δy. This has important implications. To see this, we first note that there exists an infinity of branches of spatially periodic solutions of the form

$$A = \rho\,\exp(i\Delta k\eta), \tag{47}$$

where ρ is the oscillation amplitude and Δk is a correction to the critical wave number k_c. Substituting this ansatz into Eq. (45), we obtain ρ as a function of Δy and Δk through

$$l\rho^2 + (\Delta y - \Delta k)^2 = -\Delta p + (1 - \mathcal{D})\Delta k^2. \tag{48}$$

To each value of Δk corresponds a branch of solutions and we thus have a family of curves in the bifurcation diagram, as shown in Fig. 4. A crucial observation is that the envelope of these branches is itself a branch of solutions. It is obtained by combining Eq. (48) and the constraint that $\partial\rho/\partial(\Delta k) = 0$. The latter imposes that Δk varies with Δy as

$$\Delta k = \Delta k_{env} = \frac{\Delta y}{\mathcal{D}}, \tag{49}$$

which, by substitution in Eq. (48), yields

$$l\rho_{env}^2 + \frac{\mathcal{D} - 1}{\mathcal{D}}\Delta y^2 = -\Delta p. \tag{50}$$

The amplitude of this particular solution is thus described by a conical curve in the bifurcation diagram. This curve is determined by the values of l and $\mathcal{D}$. Equation (45) shows from direct inspection that l must be positive for any periodic solution to be stable, unless, possibly, if $l \ll 1$, which we will consider later. Let us assume therefore $l > 0$ in the following (this first situation was already described in [29]). It is easy to linearize Eq. (45) around the envelope solution (50) and to verify that it is linearly stable in that case.

If $\mathcal{D} > 1$ and $\Delta p < 0$, the branches in Eq. (48) are ellipses and so is the envelope one. The latter connects the two instability points, between which the homogeneous solution is unstable. The fact that these two instability points can be connected in spite of their different characteristic wave numbers is possible on account of the dependence of Δk with Δy in Eq. (49).

The reverse situation happens when $\mathcal{D} < 1$ and $\Delta p > 0$. In this case, the homogeneous solution is stable between the two instability points. From these, two envelope branches emerge and grow in opposite directions. If, however, Δp is decreased and becomes negative while keeping $\mathcal{D} < 1$, the two instability points merge and annihilate. In this way, the two envelope branches merge so that the resulting envelope is nowhere connected to the homogeneous steady state [see Figs. 4(C) and 4(F)]. This proves the existence of *isolated* branches of solution in the semiconductor cavity. In this situation, no threshold is associated with the instability. These analytical predictions are fully confirmed by the numerical integration of the real order parameter equation (see Fig. 3 of Ref. [29]).

Let us note that, although the isolated branch exists for arbitrarily large values of the reduced injection field y, this is not the case in the original model (1) and (2). In the latter, the high-intensity branch of homogenous solution eventually regains stability through a MI point. This happens for large injection field amplitudes Y, out of the validity range of Eq. (21).

Let us now consider the limit where $l \ll 1$. This is obtained if a is close to $13/54$, in which case $\mathcal{D}$ is automatically less than 1. Equation (45) then fails to provide the amplitude of the periodic solution and an interesting higher order analysis is possible. We first set

$$a = \frac{13}{54}(1 + \bar{\epsilon}\Delta l), \tag{51}$$

where $\bar{\epsilon}$ is the same expansion parameter as before. Since p_c depends on a, Eq. (31), it effectively becomes $p_c = p_c^{(0)} + \epsilon p_c^{(1)} + \cdots$ and it is necessary to modify the expansion in Eq. (35) as

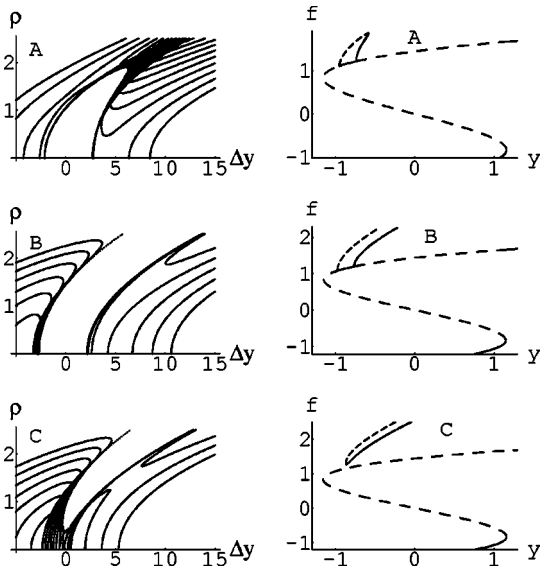

FIG. 5. Bifurcation diagrams resulting from a higher-order analysis when $a \simeq 13/54$ (see text for description).

$$p = p_c^{(0)} + \overline{\epsilon} p_c^{(1)} + 3\overline{\epsilon}^2 \Delta p. \tag{52}$$

The development for y in Eq. (26) and the slow scales (38) still hold, but the adequate expansion for the field is now

$$f = f_c + \overline{\epsilon}^{1/2} \psi_{1/2}(x,t;\eta,\sigma) + \overline{\epsilon} \psi_1(x,t;\eta,\sigma) + \cdots. \tag{53}$$

At leading order in $\overline{\epsilon}^{1/2}$, one finds $\partial \psi_{1/2}/\partial t = \mathcal{L}\psi_{1/2}$, yielding $\psi_{1/2} = A(\eta,\sigma)\exp(ik_c x) + \text{c.c.}$ The rest of the calculation is along the same lines as before and presents no particular interest. At the end of the day, we obtain a solvability condition at order $\overline{\epsilon}^{5/2}$. This yields

$$\frac{\partial A}{\partial \sigma} = A\left(r_1 + r_2|A|^2 + r_3|A|^4 + i r_4 \frac{\partial |A|^2}{\partial \eta} \right) - i(r_5 + r_6|A|^2)\frac{\partial A}{\partial \eta} + \mathcal{D}\frac{\partial^2 A}{\partial \eta^2}, \tag{54}$$

where the coefficients r_i are given by

$$r_1 = -\Delta p - \left(\frac{5}{12} k_c^2 \Delta l + \Delta y \right)^2, \quad r_2 = \frac{10}{3}\Delta l + \frac{12}{k_c^2}\Delta y,$$

$$r_3 = \frac{-23247}{676 k_c^4}, \quad r_4 = \frac{1062}{65 k_c^2}, \quad r_5 = \frac{121}{270} k_c^2 \Delta l + 2\Delta y, \tag{55}$$

$$r_6 = \frac{659}{65 k_c^2}.$$

Here, again, an infinity of periodic branches and their envelope can be obtained, in the same way as with Eq. (45). Figure 5 shows the complicated shapes that the individual branches now assume and their envelope. As can be seen in Fig. 5(A), when $\Delta l < 0$, $\Delta p < 0$, the envelope solution emerging from one of the MI points is supercritical, hence stable. This envelope branch, however, ends at a limit point, where it meets the other, unstable, envelope branch emerging from the other MI point. As Δl is progressively increased, this limit point migrates to the right of the bifurcation diagram and tends to infinity as $\Delta l \to 0^-$. For $0 < \Delta l$, the two envelope branches are disjoint [Fig. 5(B)]. From this situation, decreasing Δp induces the two MI points to merge, so that the envelope branch separates from the homogeneous solution altogether, as in Fig. 5(C). This time, however, the transition does not necessarily occurs at $\Delta p = 0$. We have thus found the connection between the different types of bifurcation diagrams encountered so far. Moreover, Fig. 5 suggests that the envelope branches in Figs. 4(E) and 4(F) do not extend indefinitely on the left. Rather, we expect that, even when l is not small, they reach a limit point and subsequently fold towards higher intensity. This is because they are formed by solutions emanating from the high-intensity state of the bistable cavity and can therefore not extend much further than the high-intensity limit point of the homogeneous steady state.

Let us remark that, in lieu of $\rho \exp i\Delta k \eta$, we could have used the family of exact solutions $A = \rho\ \text{sech}(\gamma\eta)\exp i\Delta k \eta$ and proceeded along the same line as above. This has the advantage of dealing with finite energy modulation of the field but significantly complicates the algebra.

V. DISTANT INSTABILITIES

If the two instabilities are well apart in the bifurcation diagram or if only one of them exists, then they can be studied separately. In the vicinity of either of f_+ and f_-, the solution can be written as

$$f(x,t) = f_\pm + (B_\pm(x,t)e^{ik_\pm x} + \text{c.c.}). \tag{56}$$

The modulation amplitude $B_\pm$ can be obtained by standard weakly nonlinear analysis [4,49]. One finds

$$\frac{\partial B_\pm}{\partial t} = m_1(y - y_\pm)B_\pm - m_2 B_\pm |B_\pm|^2 + m_3 \frac{\partial^2 B_\pm}{\partial x^2}, \tag{57}$$

where the coefficients m_i are given by

$$m_1 = \frac{5k_\pm^2 + 12 f_\pm}{6f_\pm^2 + 2p}, \quad m_3 = 4ak_\pm^2,$$

$$m_2 = 3 - \frac{8f_\pm^2 - 18 f_\pm k_\pm^2 + 9k_\pm^4}{(4/9)(3f_\pm^2 + 8ak_\pm^4 + p)} - \frac{72 f_\pm^2 - 42 f_\pm k_\pm^2 + 5k_\pm^4}{6f_\pm^2 + 2p}. \tag{58}$$

This amplitude equation is the only rigorous result that we can derive in the present situation. It reliably indicates whether the bifurcating branch is supercritical and stable ($m_2 > 0$) or not. However, it is only valid very close to the bifurcation point: it cannot, for instance, account for a bifurcation diagram such as the one shown in Fig. 2, where the branch of periodic solutions connects two distant bifurcation points.

In an attempt to make analytical progress, we decompose the solution in the form

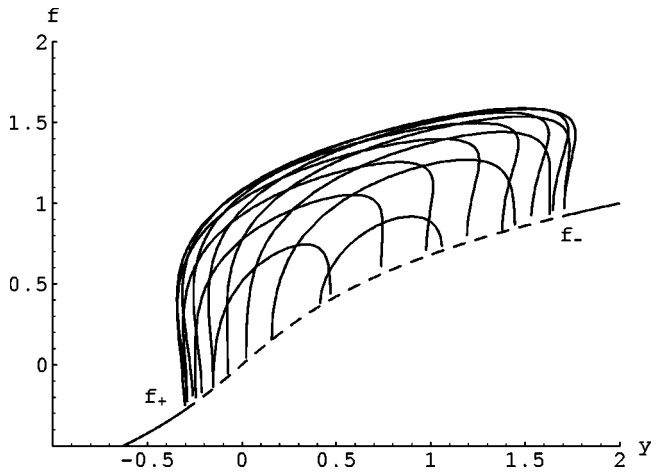

FIG. 6. Analytical bifurcation diagram for distant instabilities in one spatial dimension. The parameter values are the same as in Fig. 2. The family of periodic branches is computed from Eqs. (60) and (61).

$$f(x,t) = W_0 + (W_k e^{ikx} + \text{c.c.}). \tag{59}$$

In this ansatz, it is important to note that the "homogeneous-mode" amplitude W_0 is not fixed *a priori*. It is now coupled to W_k. This point was emphasized in [26,50,51]. The use of such a truncated Fourier decomposition is hard to justify mathematically. Still, numerical simulations indicate that the solution remains fairly harmonic in space, far from the point of instability; hence, this approach appears reasonable. It was previously applied to semiconductor cavities in [32]. We now simply substitute this ansatz into Eq. (21) and neglect higher harmonics. In the steady state, this yields the two algebraic equations

$$y = W_0(p + W_0^2) + (6W_0 - k^2)W_k^2, \tag{60}$$

$$3W_k^2 = -p - 3W_0^2 + \left(\frac{5}{2}W_0 - d\right)k^2 - ak^4. \tag{61}$$

Here again, we let the wave number k vary between the two critical values k_+ and k_-. This allows us, as before, to draw an infinity of branches in the bifurcation diagram and we focus on the envelope of these branches. The result, displayed in Fig. 6, shows a satisfying agreement with the numerical simulations.

VI. TWO-DIMENSIONAL PATTERNS

We now consider two-dimensional (2D) systems. The linear stability analysis is the same as in the one-dimensional case. The stripes have already been described in the previous section. Hence, we focus on hexagonal and honeycomb patterns. We do not consider rhombic (square) structures, because we never observed them numerically. Besides, we know that they are intrinsically unstable for the Swift-Hohenberg equation, which is a degenerate version of Eq. (21) (the proof of this statement is similar to that in [52] for tetrahedral dissipative structures). This strongly suggests that the hexagon-square transition that has been reported in other classes of nonlinear optical systems (see, for example, photorefractive feedback systems [53]) is excluded in our model. An essential difference that appears when considering the 2D problem is that wave numbers are replaced by wave vectors in the transverse plane. The homogeneous steady state is destabilized by triplets $(\mathbf{k}_1,\mathbf{k}_2,\mathbf{k}_3)$ of wave vectors which have the same modulus k and which sum to zero. The triplet itself is defined up to an arbitrary orientation in the transverse plane (rotational degeneracy). A nonlinear interaction between modes selects and stabilizes a regular pattern. In the following, we consider only the resonant interaction between transverse mode $\mathbf{k}_j$, leaving again k as a parameter, and include the effect of the quasineutral mode, as in the 1D problem. Hexagonal and honeycomb patterns correspond to the superposition of three modes with wave vectors of identical modulus and with an angle of $2\pi/3$ between them. We thus look for a solution of the form

$$f(\mathbf{x},t) = W_0 + \left[\sum_{j=1}^{3} W_k \exp\, i(\mathbf{k}_j \,.\, \mathbf{x} + \phi_j) + \text{c.c.}\right]. \tag{62}$$

By replacing this ansatz in Eq. (21) and using the truncated Fourier mode expansion we find, in the steady state, that

$$y = W_0(p + W_0^2) - 3(6W_0 + 4W_k\cos\,\psi - k^2)W_k^2 \tag{63}$$

and

$$15W_k^2 - 3(k^2 - 2W_0)\cos(\psi)W_k = -p - 3W_0^2 + \left(\frac{5}{2}W_0 - d\right)k^2 - ak^4, \tag{64}$$

where

$$\psi = \phi_1 + \phi_2 + \phi_3. \tag{65}$$

The steady-state solutions $\psi=0$ and $\psi=\pi$ give arise to hexagons and honeycombs, respectively.

The results of the above analysis are summarized in the 2D bifurcation diagram displayed in Fig. 7, where we have plotted the maximum amplitude corresponding to stripes (W_0+2W_k), hexagons (W_0+6W_k), and honeycombs (W_0+3W_k) as a function of the input field amplitude y. We used the same parameter values as in Figs. 2 and 6. Very good agreement is found with a direct numerical integration of the real order parameter equation. When increasing the control parameter y, the structures that appear first are the hexagons $(\psi=0)$. They are stable until the system exhibits transition to stripes. Further increasing the input field amplitude, the stripes become unstable and we observe the transition towards the formation of honeycomb structures $(\psi=\pi)$. There are two parameter regions where there is an overlapping domain of stability between stripes and hexagons or honeycombs. On the other hand, for the parameter values considered, hexagons and honeycombs cannot coexist. All the branches of solutions are asymmetric with respect to the point $(f=0,\ y=0)$. Finally, the bifurcation to hexagons and honeycombs can be either supercitical or subcritical. The shape of the bifurcation diagram is very similar to the one obtained numerically in [30].

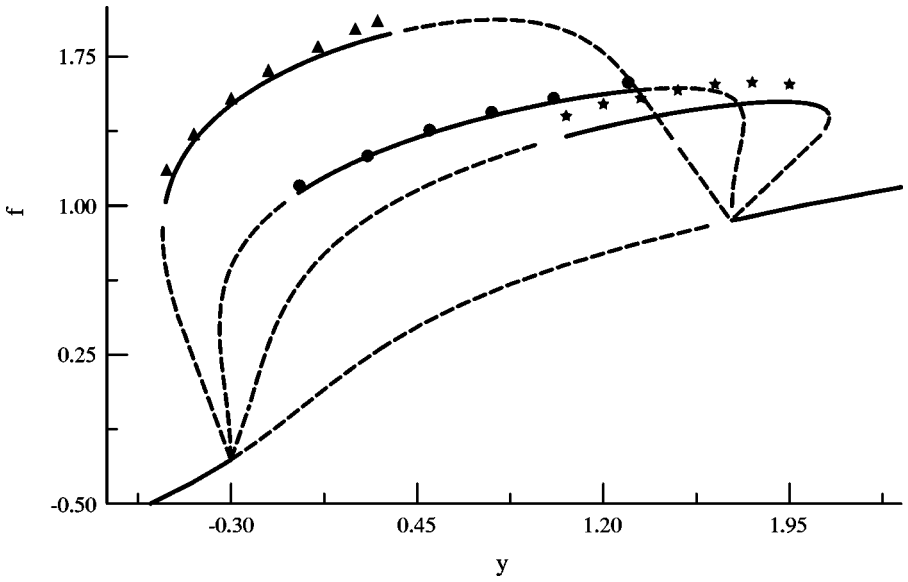

FIG. 7. Bifurcation diagram for distant instabilities in two transverse dimensions. The parameter values are the same as in Figs. 2 and 6. Symbols indicate numerically computed amplitudes for hexagons (▲), stripes (●), and honeycombs (★). As in Fig. 6, one can draw many branches of periodic solutions, each with fixed k, using Eqs. (63) and (64) with $\psi=0$ (hexagons) or $\psi=\pi$ (honeycombs). Only the envelopes of these branches are shown here. Dashed portions of the curves are numerically found to be unstable.

VII. DISCUSSION

It is well known that, at the onset of a modulational instability, a band of wave numbers becomes unstable. Accordingly, a continuous family of branches of periodic solutions is generated. In the simplest case of a single, supercritical bifurcation, it generally suffices to consider only the most unstable wave number at the instability point. However, when two MI's with different critical wave numbers are present, it is necessary to consider the whole band of unstable wave numbers in order to construct the solution that joins the two bifurcation points. In this respect, the *envelope* of the periodic branches plays a predominant role, as it emerges from the study of the normal-form equations (45) and (54). This particular branch assumes nontrivial shapes and reveals features which could hardly be anticipated by considering patterns with a fixed wave number only (see Figs. 4 and 5). The envelope branch can be viewed as the result of a continuous bifurcation process between branches of periodic solutions that have a fixed wave number. In order to have a bifurcation from one branch to the next, the two solutions must coincide to first order both in amplitude and in wave number. This can only happen on the envelope and it is through this constraint that the two instabilities interact. This is quite different from the more familiar resonant interaction between two MI's, in which some precise set of critical wave vectors belonging to either of the two MI's sums to zero. Mathematically, another sign of the interaction between the two instabilities discussed here is the fact that it is of codimension 2: two bifurcation parameters are necessary to unfold the entire bifurcation structure [48].

From a numerical point of view, the above observation may have important consequences. Recent numerical investigations of similar optical models exploited the periodicity of the solution to discretize the stationary problem on a single spatial period only [30,31]. This conveniently allows to reduce the interval on which the equation is discretized, hence to diminish the truncation error by taking a smaller space step. However, this artificially imposes the periodicity of the computed solution. As we have seen throughout this paper, the modulus k of the wave number is a quantity that naturally varies along the bifurcation diagram. The authors in [31] lucidly addressed the question of stability with respect to perturbations that do not have the periodicity of their grid. They also recognized that they could in principle find a periodic solution with any wave number by controlling the size of the elementary cell on which the equation is discretized. What the present work suggests is to adjust the size of the elementary cell so as to construct the envelope branch. This is confirmed in Fig. 2, where the bifurcation diagram of the real order parameter equation (21) was compared to the original model. On the one hand, we integrated the time-independent, one-dimensional version of Eq. (21) on an elementary cell with periodic boundary conditions. For each point of the bifurcation diagram, we adjusted the spatial period so as to extremize the amplitude of the solution. On the other hand, we integrated the time-dependent original model (1) and (2) on a much larger domain, letting the system dynamically select the wave number. The solution dynamically evolved towards the envelope branch. This agrees with the stability predictions from the normal-form equation (45).

Concerning the isolated branch of solutions shown in Fig. 3 of [29], it has no bifurcation, hence no threshold associated with it. It is, however, formed by solutions that bifurcate from an unstable portion of the high-intensity homogeneous branch [Fig. 4(F)]. Therefore, it does not correspond to the experimental observation of thresholdless hexagons [35], which are found at low intensities and with a linearly stable background. Let us point out, however, that the normal forms (45) and (54) can in principle describe isolated branches of solution on a *stable* homogeneous background. Assume for example that $l<0$, $\mathcal{D}>1$, and $\Delta p>0$ in Eq. (50). In this case, there exists a family of isolated branches of periodic solutions despite the complete absence of MI's. Admittedly, these solutions would be unstable in the frame of the cubic Ginzburg-Landau equation (45); moreover, the conditions on l and $\mathcal{D}$ for such a scenario cannot simultaneously be met in the nascent bistability limit with zero cavity detuning. However, stability can potentially be recovered within the quintic Ginzburg-Landau description (54). Besides, the form of Eqs.

(45) and (54) is general and can be derived from the original model, independently of nascent bistability. Further investigations are necessary to clarify this point but it seems clear that a thresholdless phenomenon such as the one reported in [35] does not necessarily stem from device imperfections.

Finally, we would like to mention that vegetation patterns are governed by equations very similar to the real order parameter equation derived here. Semi-arid environments have been described in the weak phytomass density ρ and weak gradient limits [39]. This leads to a logisticlike equation containing a nonlinear diffusive term of the form $(L-\rho)\nabla^2\rho$. Such a term accounts for the positive effect that established plants can have on the growth of other plants — e.g., by producing shadow, littering nutrients, and protecting against herbivores. Because of this nonlinear diffusion, these ecosystems can potentially be destabilized by MI's with different critical wave numbers. They are thus liable to produce some of the bifurcation zoology described in this paper.

The authors are grateful to S.J. Chapman and J.R. Ockendon for their illuminating comments. G.K. was supported by EU TMR Grant No. FMRXCT 97011 [HBKEY]. M.T. received support from the Fonds National de la Recherche Scientifique (Belgium). This work was also partially supported by the Interuniversity Attraction Pole program of the Belgian government.

[1] P. Glansdorff and I. Prigogine, *Thermodynamics of Structures, Stability and Fluctuations* (Wiley, New York, 1971).
[2] G. Nicolis and I. Prigogine, *Self-organization in Nonequilibrium Systems* (Wiley, New York, 1977).
[3] H. Haken, *Synergetics: An introduction* (Wiley, New York, 1978).
[4] M. C. Cross and P. C. Hohenberg, Rev. Mod. Phys. **65**, 851 (1993).
[5] D. Walgraef, *Spatio-Temporal Pattern Formation* (Springer, Berlin, 1997).
[6] L. M. Pismen, *Vortices in Nonlinear Fields* (Oxford University Press, Oxford, 1998).
[7] N. N. Rosanov and Semenov, Opt. Spectrosc. **48**, 59 (1980).
[8] J. V. Moloney and H. M. Gibbs, Phys. Rev. Lett. **48**, 1607 (1982).
[9] L. A. Lugiato and R. Lefever, Phys. Rev. Lett. **58**, 2209 (1987).
[10] A. M. Turing, Philos. Trans. R. Soc. London, Ser. B **327**, 37 (1952); I. Prigogine and R. Lefever, J. Chem. Phys. **38**, 1659 (1968).
[11] M. Santagiustina, P. Colet, M. San Miguel, and D. Walgraef, Phys. Rev. Lett. **79**, 3633 (1997); M. Taki, M. San Miguel, and M. Santagiustina, Phys. Rev. E **61**, 2133 (2000); H. Ward, M. Taki, and P. Glorieux, Opt. Lett. **27**, 348 (2002).
[12] S. Coen, M. Tlidi, Ph. Emplit, and M. Haelterman, Phys. Rev. Lett. **83**, 2328 (1999).
[13] M. Le Berre, A. S. Patrascu, E. Ressayre, and A. Tallet, Phys. Rev. A **56**, 3150 (1997); M. Le Berre, E. Ressayre, and A. Tallet, J. Opt. **1**, 153 (1999); M. Tlidi, M. Le Berre, E. Ressayre, A. Tallet, and L. Di Menza, Phys. Rev. A **61**, 043806 (2000).
[14] A. C. Newell and J. V. Moloney, *Nonlinear Optics* (Addison-Wesley, Redwood City, CA, 1992).
[15] L. A. Lugiato, Chaos, Solitons Fractals **4**, 1264 (1994).
[16] N. N. Rosanov, *Progress in Optics* (North-Holland, Amsterdam, 1996), Vol. 35; *Spatial Hysteresis and Optical Patterns* (Springer, Berlin, 2002).
[17] A. Buka and L. Kramer, *Pattern Formation in Liquid Crystals* (Springer-Verlag, New York, 1996).
[18] P. Mandel, *Theoretical Problems in Cavity Nonlinear Optics* (Cambridge University Press, Cambridge, England, 1997).
[19] G. de Valcarcel, E. Roldan, and R. Vilaseca, Quantum Semiclassic. Opt. **10**, 775 (1998); see also the special issue on the subject, J. Opt. B: Quantum Semiclassical Opt. **1**, (1999).
[20] L. A. Lugiato, M. Brambilla, and A. Gatti, Adv. At., Mol., Opt. Phys. **40**, 229 (1998).
[21] F. T. Arecchi, S. Boccaletti, and P. L. Ramazza, Phys. Rep. **318**, 1 (1999).
[22] R. Neubecker and T. Tschudi, Chaos, Solitons Fractals **10**, 615 (1999).
[23] W. Lange and T. Ackemann, J. Opt. Soc. Am. B **2**, 347 (2000).
[24] K. Staliunas and V. J. Sanchez-Morcillo, *Transverse Patterns in Nonlinear Optical Resonators*, Springer Tracts in Modern Physics (Springer-Verlag, Berlin, 2003).
[25] M. Tlidi and M. Haelterman, Phys. Lett. A **239**, 59 (1998); M. Tlidi, P. Mandel, and M. Haelterman, Phys. Rev. E **56**, 6524 (1997).
[26] M. Tlidi, A. G. Vladimirov, and P. Mandel, IEEE J. Quantum Electron. **39**, 216 (2003).
[27] M. Tlidi and M. Taki, Phys. Rev. Lett. **91**, 023901 (2003).
[28] S. Coen and M. Haelteman, Opt. Lett. **24**, 80 (1999).
[29] G. Kozyreff, S. J. Chapman, and M. Tlidi, Phys. Rev. E **68**, 015201(R) (2003).
[30] T. Maggipinto, M. Brambilla, and W. J. Firth, IEEE J. Quantum Electron. **39**, 206 (2003).
[31] G. K Harkness, W. J. Firth, G.-L. Oppo, and J. M. McSloy, Phys. Rev. E **66**, 046605 (2002); **66**, 046606 (2002).
[32] D. Michaelis, U. Peschel, and F. Lederer, Phys. Rev. A **56**, R3366 (1997).
[33] M. Brambilla, L. A. Lugiato, F. Prati, L. Spinelli, and W. J. Firth, Phys. Rev. Lett. **79**, 2042 (1997); L. Spinelli, G. Tissoni, M. Brambilla, F. Prati, and L. A. Lugiato, Phys. Rev. A **58**, 2542 (1998).
[34] G. Tissoni, L. Spinelli, M. Brambilla, T. Maggipinto, I. M. Perrini, and L. A. Lugiato, J. Opt. Soc. Am. B **16**, 2083 (1999); **16**, 2095 (1999); L. Spinelli, G. Tissoni, M. Tarenghi, and M. Brambilla, Eur. Phys. J. D **15**, 257 (2001).
[35] V. B. Taranenko, I. Ganne, R. J. Kuszelewicz, and C. O. Weiss, Phys. Rev. A **61**, 063818 (2000); V. B. Taranenko, C. O. Weiss, and B. Schapers, *ibid.* **65**, 013812 (2001); R. Kuszelewicz, I. Ganne, I. Sagnes, G. Slekys, and M. Brambilla, Phys. Rev. Lett. **84**, 6006 (2000); V. B. Taranenko, I. Ganne, R. J. Kuszelewicz, and C. O. Weiss, Appl. Phys. B: Lasers Opt. **72**, 377 (2001).

[36] S. Barland, J. R. Tredicci, M. Brambilla, L. A. Lugiato, S. Balle, M. Guidici, T. Maggipinto, L. Spinelli, G. Tissoni, T. Knodl, M. Miller, and R. Jager, Nature (London) **419**, 699 (2002).

[37] M. Tlidi, P. Mandel, and R. Lefever, Phys. Rev. Lett. **73**, 640 (1994); W. J. Firth and A. J. Scroggie, *ibid.* **76**, 1623 (1996); M. Brambilla, L. A. Lugiato, and M. Stefani, Europhys. Lett. **34**, 109 (1996).

[38] T. Maggipinto, M. Brambilla, G. K. Harkness, and W. J. Firth, Phys. Rev. E **62**, 8726 (2000).

[39] R. Lefever and O. Lejeune, Bull. Math. Biol. **59**, 263 (1997); J. von Hardenberg, E. Meron, M. Shachak, and Y. Zarmi, Phys. Rev. Lett. **87**, 198101 (2001); O. Lejeune, M. Tlidi, and P. Couteron, Phys. Rev. E **66**, 010901(R) (2003).

[40] P. Mandel, M. Georgiou, and T. Erneux, Phys. Rev. A **47**, 4277 (1993).

[41] J. Lega, J. V. Moloney, and A. C. Newell, Phys. Rev. Lett. **73**, 2978 (1994); S. Longhi and A. Geraci, Phys. Rev. A **54**, 4581 (1996); A. Barsella, C. Lepers, M. Taki, and P. Glorieux, J. Opt. B: Quantum Semiclassical Opt. **1**, 64 (1999).

[42] G. J. de Valcarcel, K. Staliunas, E. Roldan, and V. J. Sanchez-Morcillo, Phys. Rev. A **54**, 1609 (1996).

[43] G. Kozyreff, M. Tlidi, P. Ramazza, and U. Bortolozzo (unpublished); M. Leclerc (unpublished).

[44] W. S. Edwards and S. Fauve, Phys. Rev. E **47**, R788 (1993); H. W. Müller, *ibid.* **49**, 1273 (1994); D. Leduc, M. Le Berre, E. Ressayre, and A. Tallet, Phys. Rev. A **53**, 1072 (1996); E. Pampaloni, S. Residori, S. Soria, and F. T. Arecchi, Phys. Rev. Lett. **78**, 1042 (1997); Z. H. Musslimani and L. M. Pismen, Phys. Rev. E **62**, 389 (2000); M. Bachir, S. Métens, P. Borckmans, and G. Dewel, Europhys. Lett. **54**, 612 (2000); G. Dewel, M. Bachir, S. Métens, and P. Borckmans, Faraday Discuss. **120**, 421 (2001); L. Yang, M. Dolnik, A. M. Zhabotinsky, and I. R. Epstein, Phys. Rev. Lett. **88**, 208303 (2002).

[45] V. J. Sanchez-Morcillo, G. J. de Valcarcel, E. Roldan, and K. Staliunas, Phys. Rev. E **57**, R4911 (1998); Phys. Rev. A **56**, 3237 (1997).

[46] V. J. Sanchez-Morcillo and G. J. de Valcarcel, Phys. Lett. A **246**, 293 (1998).

[47] H. S. Greenside and M. C. Cross, Phys. Rev. A **31**, 2492 (1985).

[48] J. Guckenheimer and P. Holmes, *Nonlinear Oscillations, Dynamical Systems, and Bifurcation of Vector Fields* (Springer-Verlag, New York, 1983).

[49] A. C. Newell and J. A. Whitehead, J. Fluid Mech. **38**, 279 (1969); L. A. Segel, *ibid.* **38**, 203 (1969).

[50] B. A. Malomed, Phys. Rev. A **45**, 1009 (1992).

[51] G. Dewel, S. Métens, M'F. Hilali, P. Borckmans, and C. B. Price, Phys. Rev. Lett. **74**, 4647 (1995).

[52] M. Tlidi, M'F Hilali, and P. Mandel, Europhys. Lett. **55**, 26 (2001).

[53] O. Sandfuchs, F. Kaiser, and M. R. Belić, Phys. Rev. A **64**, 063809 (2001).